Electronic Supplementary Material (ESI) for ChemComm.

A Low-Coordinate Iron Organoazide Complex

Andres Gonzalez,[a] Serhiy Demeshko,[b] Franc Meyer,[b] C. Gunnar Werncke[a,*]

[a]Philipps-University Marburg, Hans-Meerwein-Straße 4, D-35032 Marburg, Germany. [b]Institute of Inorganic Chemistry, University of Göttingen, Tammannstr. 4, D-37077 Göttingen, Germany

Content

General considerations

All manipulations were carried out under inert atmosphere. Compounds that required constant and precise handling were stored in a SYSTEMTECHNIK GS glovebox-system GS043818 under inert atmosphere. Solvents were dried by continuous distillation over sodium metal for several days, degassed *via* three freeze-pump cycles, and stored over 4 Å molecular sieves. Spectral analysis for ^{1}H NMR were conducted using automatic *BRUKER AV II 300 MHz* Spectrometers. The residual signals for deuterated solvents were used to calibrate the measured spectra. All measurements were carried out between 290 and 300 K. The internal standard values for ^{1}H NMR correspond to tetramethylsilane (TMS, 0.00 ppm) and the observed shifts are relative to the standard. The fit of the NMR titration curve was performed using bindfit.[1,2] Elemental analysis measurements were performed by the spectrometry team of the Philipps-University Marburg, Germany, using an *ELEMENTAR vario Micro cube* in CHN mode. Infrared spectra were recorded with a *BRUKER ALPHA FT-IR*. Classification of the signals is as follows: *w*: weak, *m*: medium, *s*: strong. The UV/Vis spectra were measured in *n*-pentane using an *ANALYTIK-JENA SPECORD S 600* spectrometer in the range from 1000 nm up to 250 nm. Solution magnetic susceptibilities were determined by the EVANS method.[3,4] $[Fe(N(SiMe_3)_2)_2]$[5] and *tert*-butylazide[6] were synthesized following literature procedures. KC_8 was obtained by heating potassium metal with stoichiometric amounts of graphite using a heat gun.

EXPERIMENTAL SECTION

[Fe{$N_3{}^tBu$}$(N(SiMe_3)_2)_2$] (**1**). $[Fe(N(SiMe_3)_2)_2]$ (100 mg, 0.265 mmol, 1 equiv.) was dissolved in *n*-pentane (1 mL) to give a light green solution. The solution was cooled down to −30 °C and added to $N_3{}^tBu$ (26.27 mg, 0.265 mmol, 1 equiv.) resulting in a light-yellow coloration. After 5 minutes at room temperature, the yellowish-green solution was stored at −30 °C overnight. [Fe{$N_3{}^tBu$}$(N(SiMe_3)_2)_2$], **1**, was obtained as colourless crystalline blocks. Yield: 82 mg (0.172 mmol, 65 %). ^{1}H-NMR (293 K, 500 MHz, toluene-d_8, ppm) δ: 35.27 (*bs*, 36 H, –Si$(CH_3)_3$), –10.40 (*bs*, 9H, –NC$(CH_3)_3$). IR (ATR, cm^{-1}): $\tilde{\nu}$ = 2946 (m), 2894 (vw), 2117 (s, azide stretching band), 1465 (vw), 1433 (vw), 1401 (vw), 1374 (w), 1283 (s), 1240 (m), 1197 (m), 960 (vs), 888 (m), 813 (vs), 786 (vs), 749 (s), 706 (m), 665 (s), 633 (m), 611 (m), 586 (m), 555 (w). Elemental analysis gave consistent substantial deviations (approx. 1% too low for carbon C, approx. 5% too low for N) despite repeated attempts. These values approach that of $Fe(N(SiMe_3)_2)_2$, yet **1** was substantiated by proton NMR, IR and Mössbauer spectroscopy, and X-Ray diffraction on large crystalline blocks, that were also used for elemental analysis.

[Fe(κ^2-*N*-N$(SiMe_3)SiMe_2CH_2$-NH^{t}Bu)$(N(SiMe_3)_2)$] (**2**). $[Fe(N(SiMe_3)_2)_2]$ (100 mg, 0.265 mmol, 1 equiv.) was dissolved in *n*-heptane to give a light green solution. The solution was cooled down to −30 °C and added to $N_3{}^tBu$ (26.27 mg, 0.265 mmol, 1 equiv.) resulting in a light-yellow coloration. The mixture was heated to 60 °C for 20 minutes, which resulted in a colour change to dark brown. The solution was concentrated and stored at −30 °C for several days. [Fe(κ^2-*N*-N$(SiMe_3)SiMe_2CH_2$-NH^{t}Bu)$(N(SiMe_3)_2)$], **2**, was obtained as pale yellow crystalline plates. Yield: 40 mg (0.09 mmol, 34 %). ^{1}H-NMR (300 K, 300 MHz, C_6D_6, ppm) δ: 72.45 (*bs*, 3 H), 69.81 (*bs*, 3 H), −1.29 (*bs*, 18 H), −7.32 (*bs*, 9 H), −11.53 (*bs*, 9 H). Magnetic susceptibility (500 MHz, 300 K, C_6D_6 + 1% TMS): μ_{eff} = 4.75 μ_B, $\mu_{S.O.}$ (S = 2) = 4.89 μ_B. IR (ATR, cm^{-1}): $\tilde{\nu}$ = 2947 (m), 2894 (w), 1477 (vw), 1431 (vw), 1412 (vw), 1392 (vw), 1370 (w), 1242 (s), 1202 (w), 1173 (w), 1037 (vw), 1008 (vs), 885 (m), 875 (m), 814 (vs), 794 (vs), 780 (vs), 749 (s), 696 (m), 667 (s), 633 (m), 626 (m), 610 (m), 503 (w). Elemental analysis: Calcd. (%) for $C_{16}H_{45}FeN_3Si_4$ (475.76 g mol^{-1}): C: 42.92, H: 10.13, N: 9.39; found: C: 42.52, H: 9.79, N: 9.44.

[($\{Me_3Si\}_2$N)Fe{μ-N^{t}Bu-μ-(N$\{SiMe_3\}_2$)Fe(N$\{SiMe_3\}_2$)] (**3**). $[Fe(N(SiMe_3)_2)_2]$ (100 mg, 0.265 mmol, 1 equiv.) was dissolved in *n*-pentane (1 mL) to give a light green solution. The solution was cooled down to −30 °C and added to $N_3{}^tBu$ (26.3 mg, 0.265 mmol, 1 equiv.) resulting in a light-yellow coloration. KC_8 (42.3 mg, 0.318 mmol, 1.2 equiv.) was added to result in gas evolution and change of colour to dark orange. After 10 minutes at room temperature, the solution was filtered and stored at −30 °C overnight. [($\{Me_3Si\}_2$N)Fe{μ-N^{t}Bu-μ-(N$\{SiMe_3\}_2$)Fe(N$\{SiMe_3\}_2$)], **3**, was obtained as dark orange blocks. Yield: 33 mg (0.047 mmol, 53 %, based on the formation of one equivalent of K($Fe(NR_2)_3$) as the by-product). ^{1}H-NMR (300 K, 300 MHz, toluene-d_8, ppm) δ: –2.41 (*bs*), −6.71 (*bs*). IR (ATR, cm^{-1}): $\tilde{\nu}$ = 2945 (m), 2890 (w), 1241 (s), 1213 (m), 982 (vs), 888 (s), 833 (vs), 782 (s), 749 (s), 711 (m), 659 (s), 609 (m), 611 (m).

Elemental analysis provided consistently deviating values for carbon and nitrogen, which we attribute to incomplete combustion and silicon carbide formation, as also the side-product K($Fe(NR_2)_3$] exhibits similar values as **3**.

Spectra of Compounds 1-3

Compound [Fe{$N_3{}^t$Bu}($N(SiMe_3)_2)_2$], 1

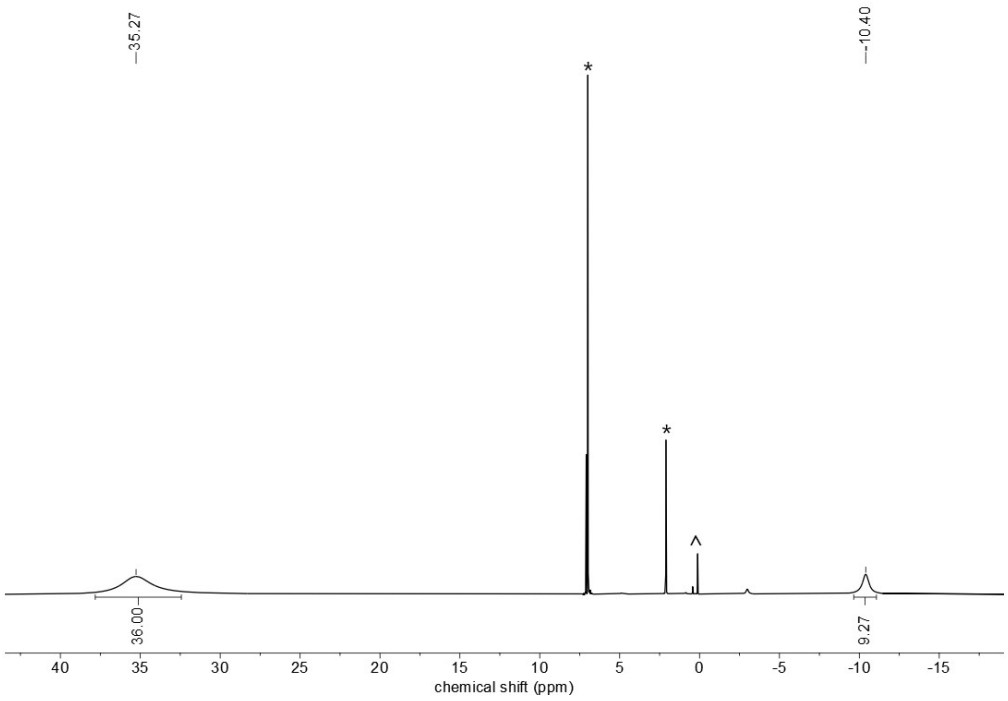

Figure S 1. ^{1}H NMR spectrum (500 MHz, 293 K, toluene-d_8) of [Fe{$N_3{}^t$Bu}($N(SiMe_3)_2)_2$], **1** (* toluene-d_8, ^ decomposition).

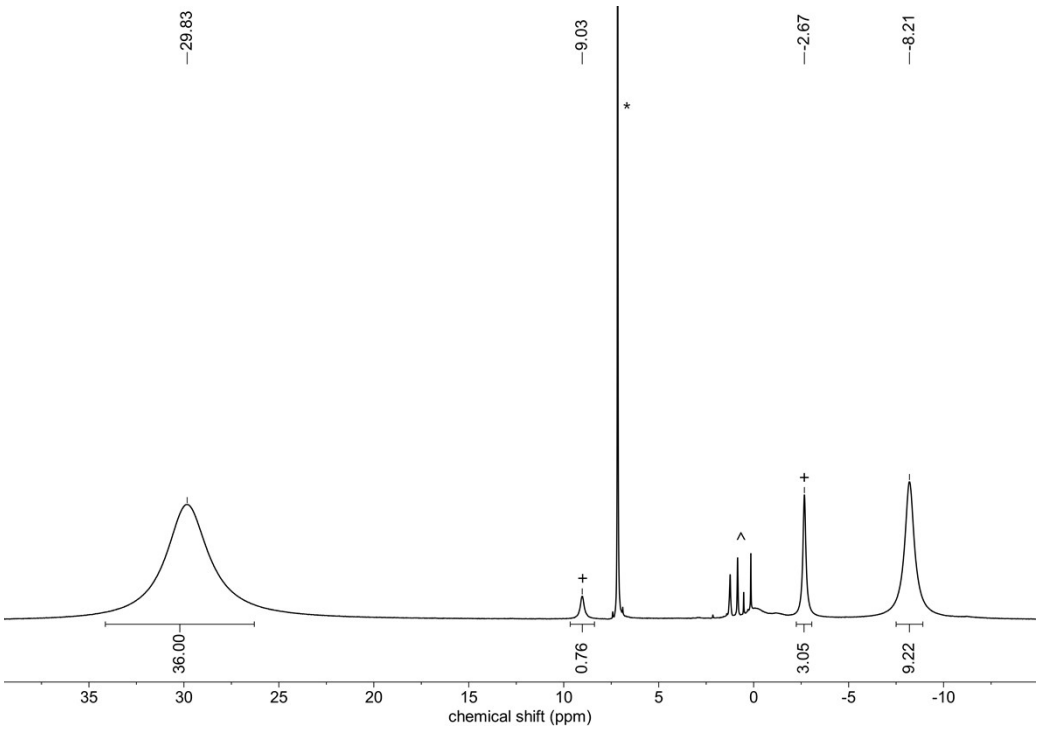

Figure S 2. ^{1}H NMR spectrum (300 MHz, 300 K, C_6D_6) of the reaction between [$Fe(N(SiMe_3)_2)_2$] and ^{t}BuN_3 after 20 min in neat conditions (* C_6D_6, + presumed imido species [**A**], ^ decomposition).

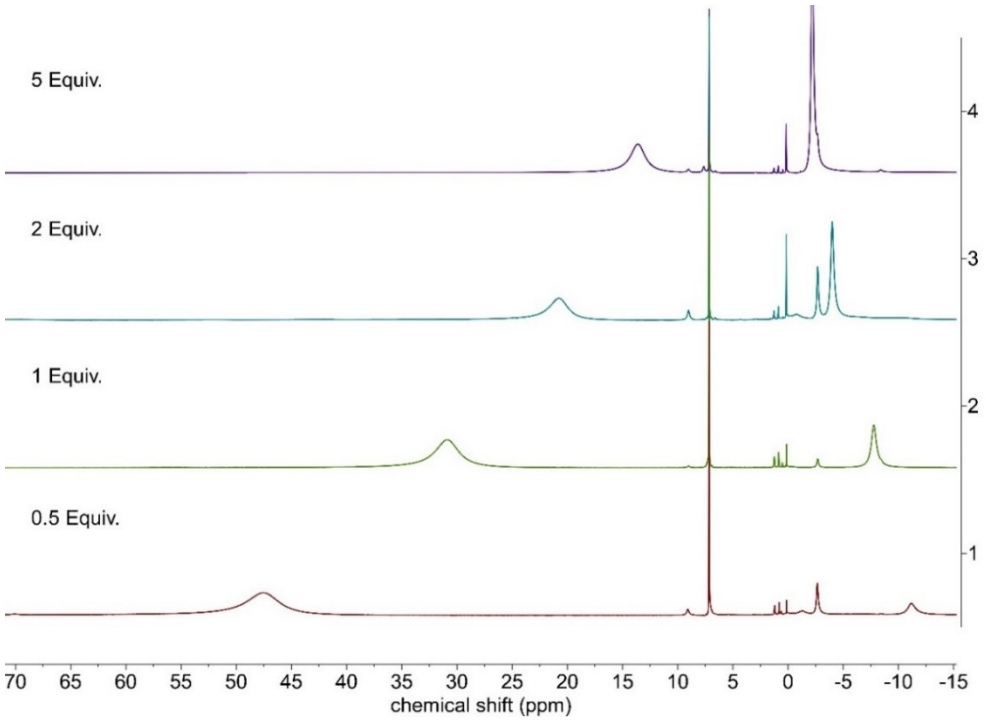

Figure S 3. ^{1}H NMR (300 MHz, 300 K, C_6D_6) study of the interaction of $[Fe(N(SiMe_3)_2)_2]$ with various amounts of $^{t}BuN_3$.

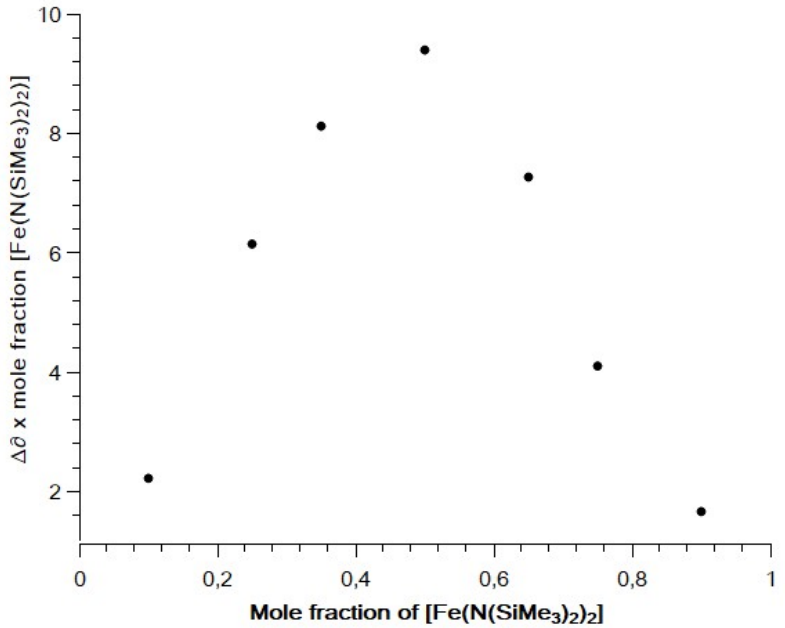

Figure S 4. Job plot showing the 1:1 adduct formation of $^{t}BuN_3$ with $[Fe(N(SiMe_3)_2)_2)]$ to give **1**.

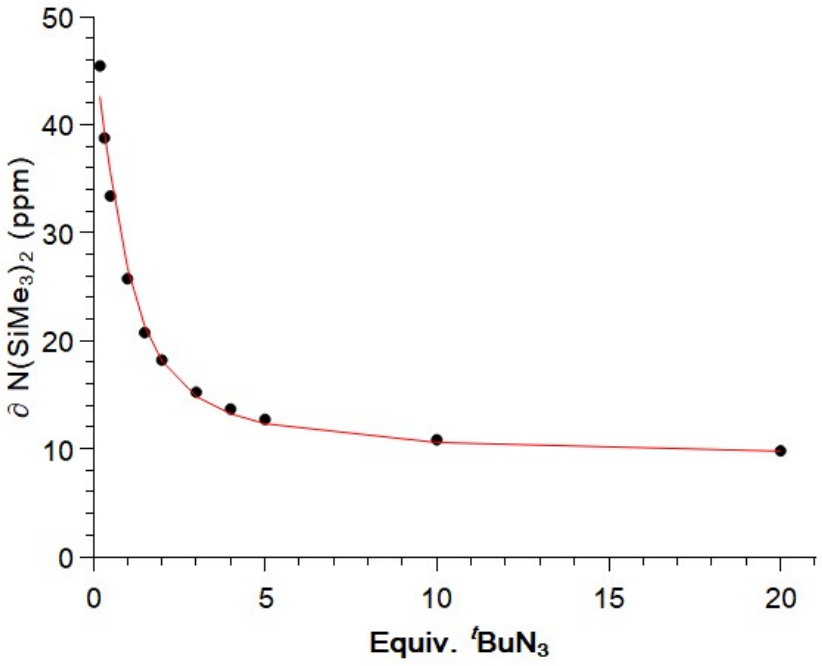

Figure S 5. Dependence of the chemical shift of the $N(SiMe_3)_2$ signal with $^tBuN_3$ equivalents, red line represents the fit obtained with bindfit (c_{FeNR2} = 0.075 M). K_{eq} = 35 (±8) M^{-1} (L-BFGS-B Method).

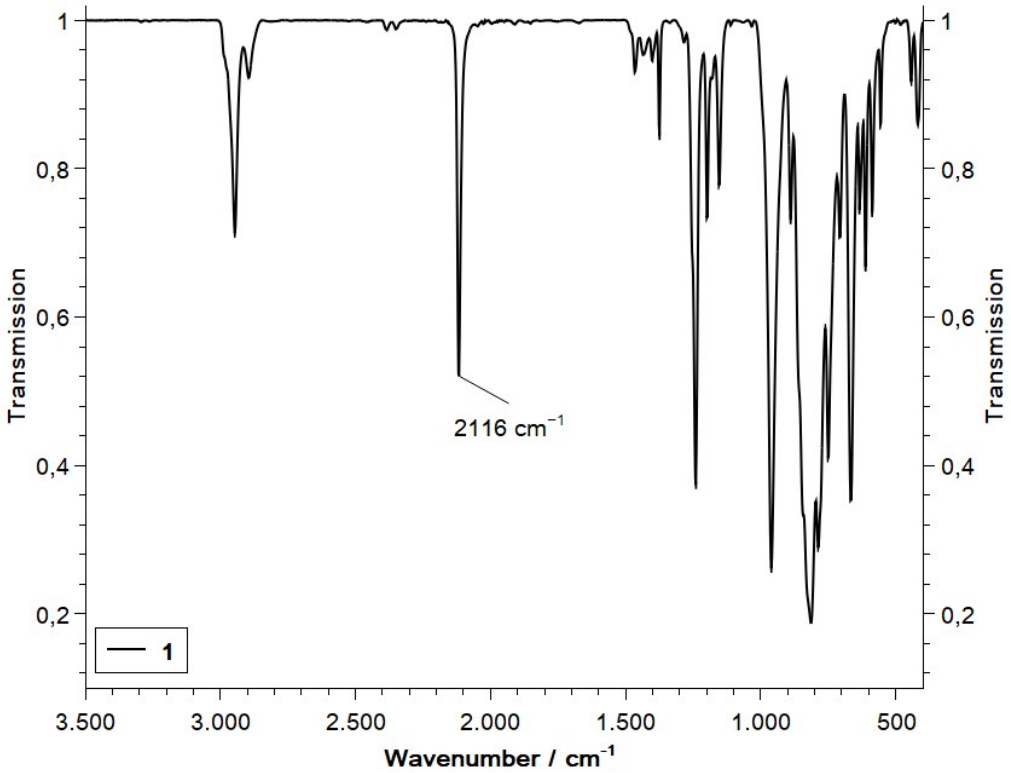

Figure S 6. ATR IR spectrum of solid $[Fe\{N_3{}^tBu\}(N(SiMe_3)_2)_2]$, **1.**

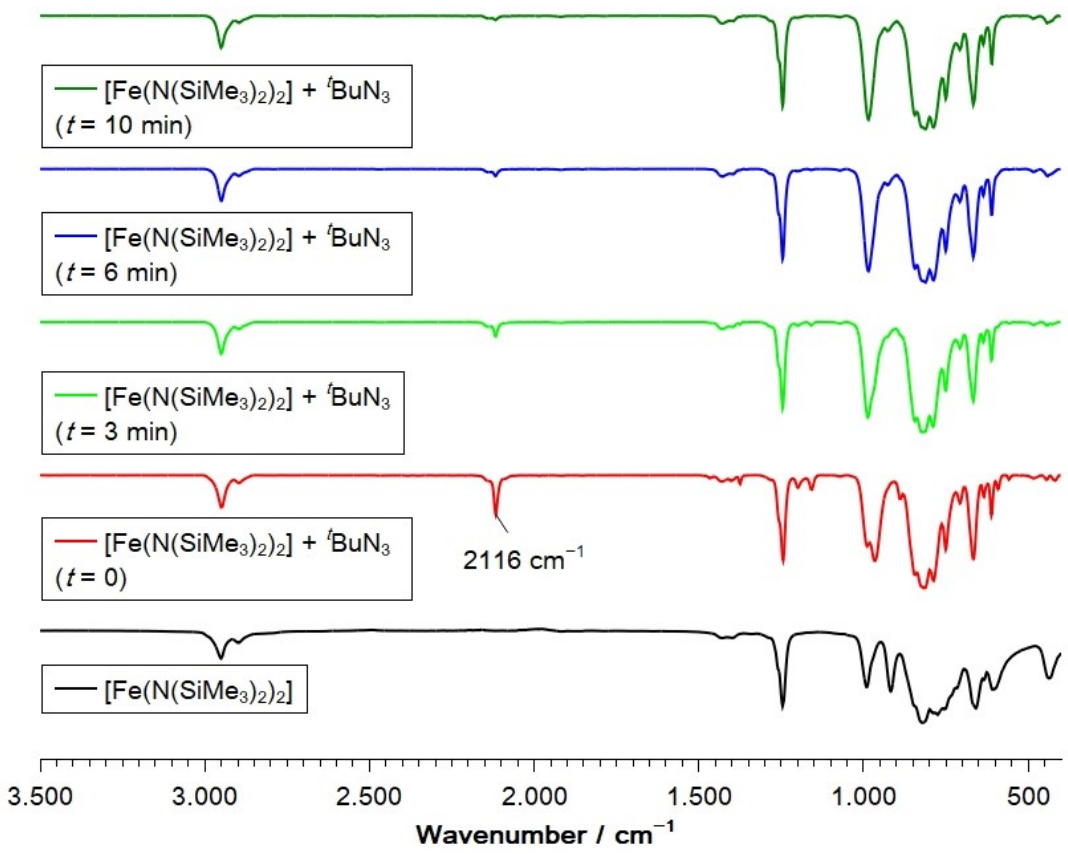

Figure S 7. ATR IR spectroscopic study of the reaction between solid $[Fe(N(SiMe_3)_2)_2]$ and $^tBuN_3$ over 10 minutes.

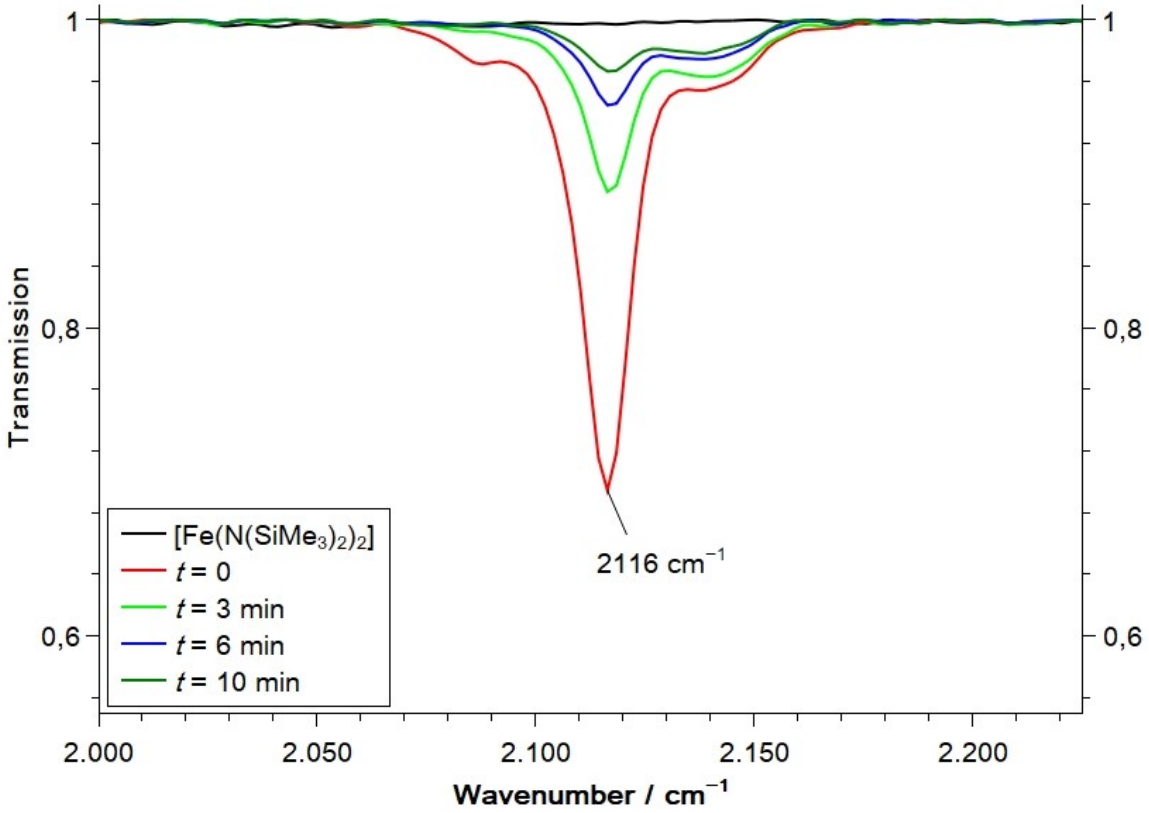

Figure S 8. Close up (2000 – 2225 cm^{-1}) of the ATR IR spectroscopic study of the reaction between solid $[Fe(N(SiMe_3)_2)_2]$ and $^tBuN_3$. The residual signal at t = 10 minutes corresponds to the slight excess of used organic azide.

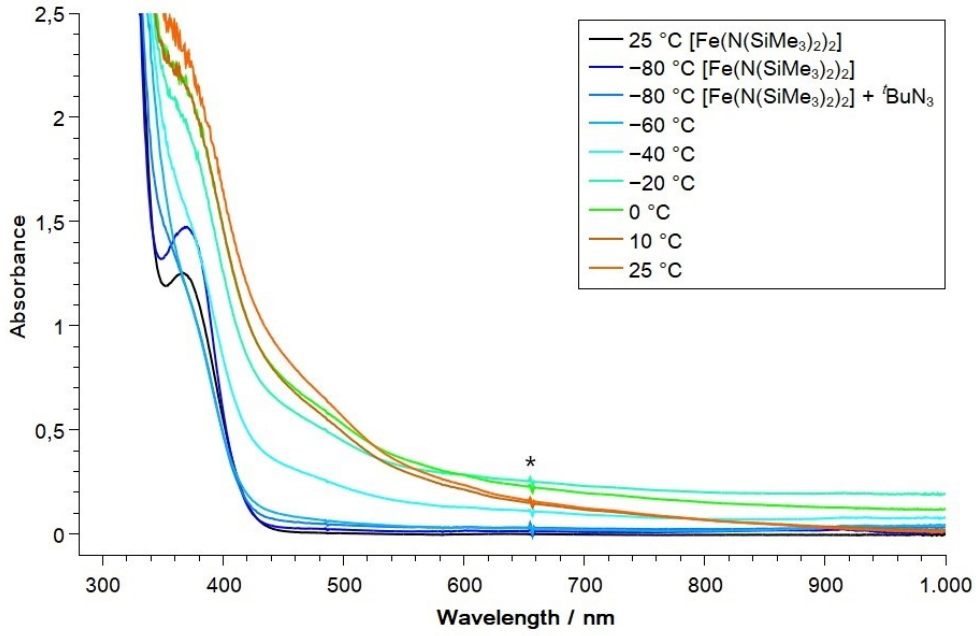

Figure S 9. Comparison of the temperature-dependent UV/Vis spectroscopic behaviour of **1** (obtained by mixing $Fe(NR_2)_2$ and $N_3{}^tBu$) with that of pure $Fe(NR_2)_2$ (shown for 25 °C and 80 °C) in *n*-pentane (* signal caused by lamp change).

Spectra of [Fe(κ²*N*-N(SiMe$_3$)SiMe$_2$CH$_2$-NH^{t}Bu)(N(SiMe$_3$)$_2$)], 2.

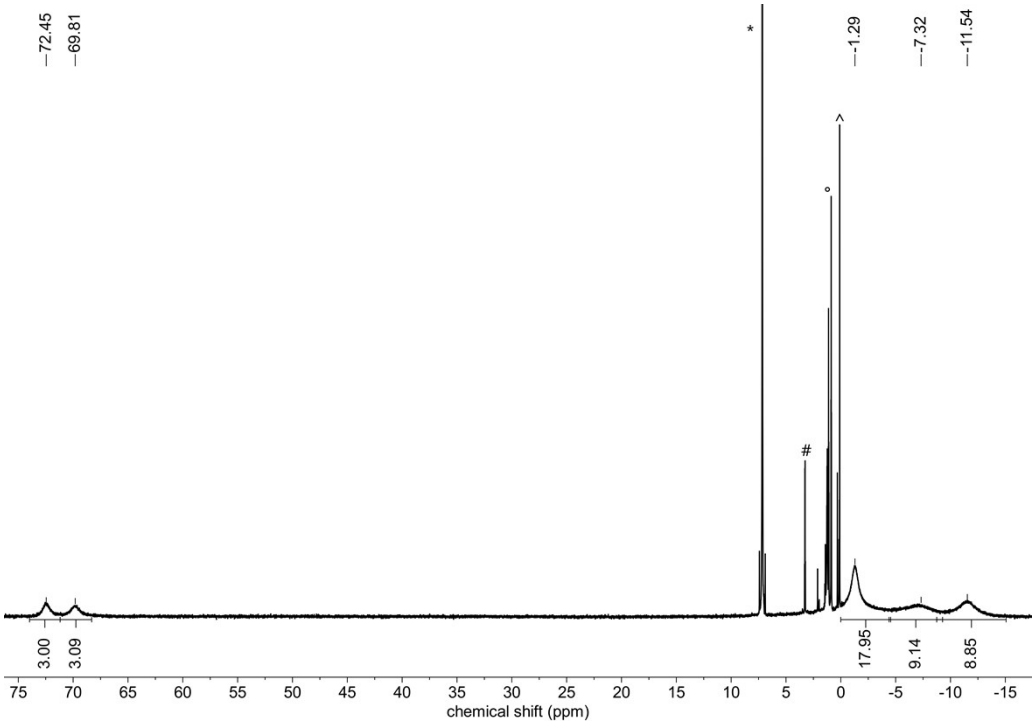

Figure S 10. ^{1}H NMR spectrum (300 MHz, 300 K, benzene-d$_6$) of [Fe(κ²N-N(SiMe$_3$)SiMe$_2$CH$_2$-NH^{t}Bu)(N(SiMe$_3$)$_2$)], **2** (* benzene-d$_6$, ° *n*-heptane, # diethyl ether, ^ decomposition).

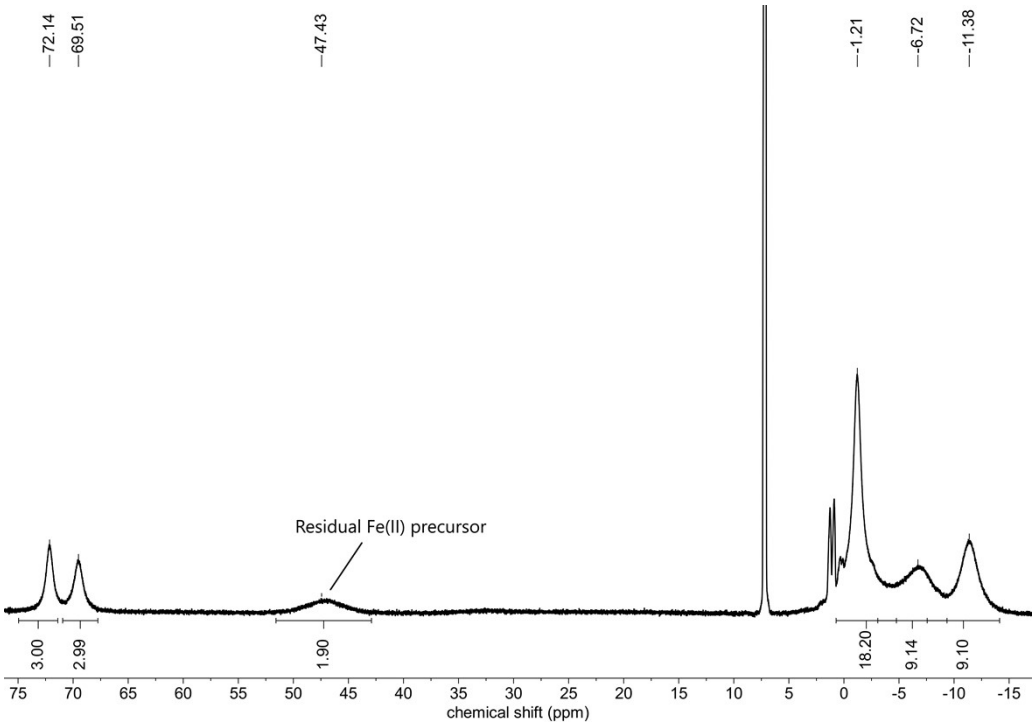

Figure S 11. ^{1}H NMR spectrum (300 MHz, 300 K, benzene-d$_6$) of crude [Fe(κ²N-N(SiMe$_3$)SiMe$_2$CH$_2$-NH^{t}Bu)(N(SiMe$_3$)$_2$)], **2**. Comparison with the residual Fe(NR$_2$)$_2$ signal indicates 95% conversion.

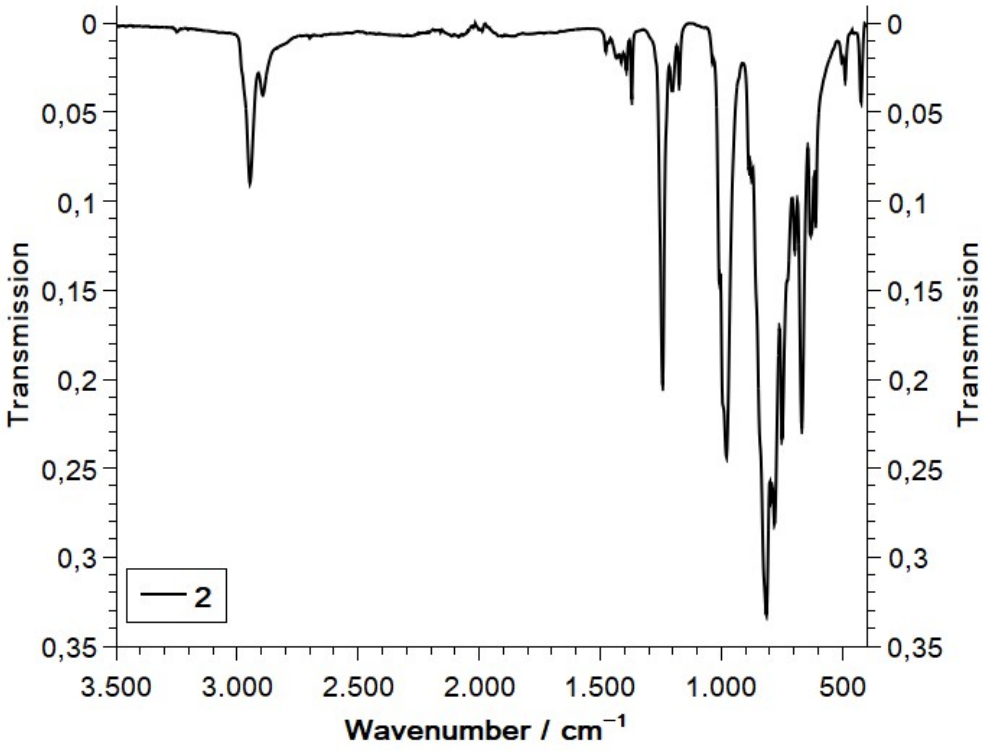

Figure S 12. ATR IR spectrum of solid [Fe(κ^2N-N(SiMe$_3$)SiMe$_2$CH$_2$-NH^{t}Bu)(N(SiMe$_3$)$_2$)], **2**.

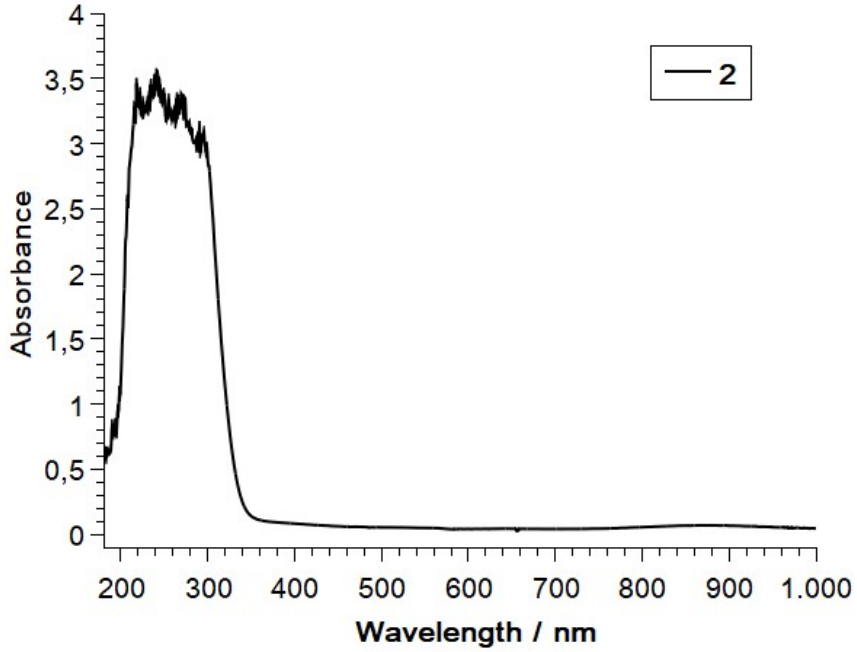

Figure S 13. UV-Vis spectrum of [Fe(κ^2N-N(SiMe$_3$)SiMe$_2$CH$_2$-NH^{t}Bu)(N(SiMe$_3$)$_2$)], **2**, in *n*-pentane.

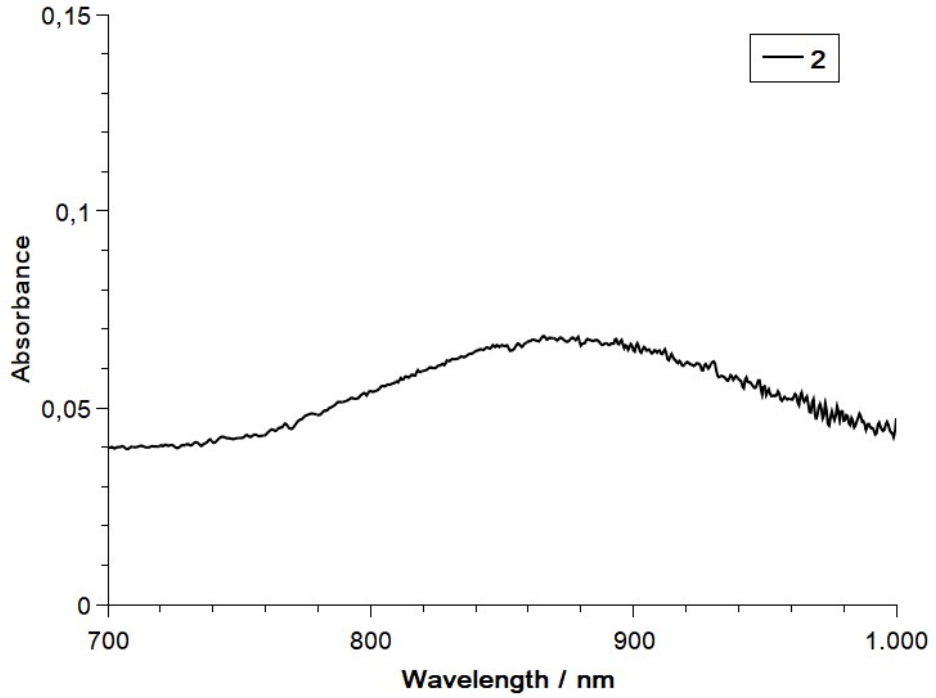

Figure S 14. Close-up UV-Vis spectrum of [Fe(κ^2N-N(SiMe$_3$)SiMe$_2$CH$_2$-NH^{t}Bu)(N(SiMe$_3$)$_2$)], **2**, in *n*-pentane in the range of 700–1000 nm.

Spectra of [({Me$_3$Si}$_2$N)Fe{μ-N^{t}Bu-μ-(N{SiMe$_3$}$_2$)Fe(N{SiMe$_3$}$_2$)] (3)

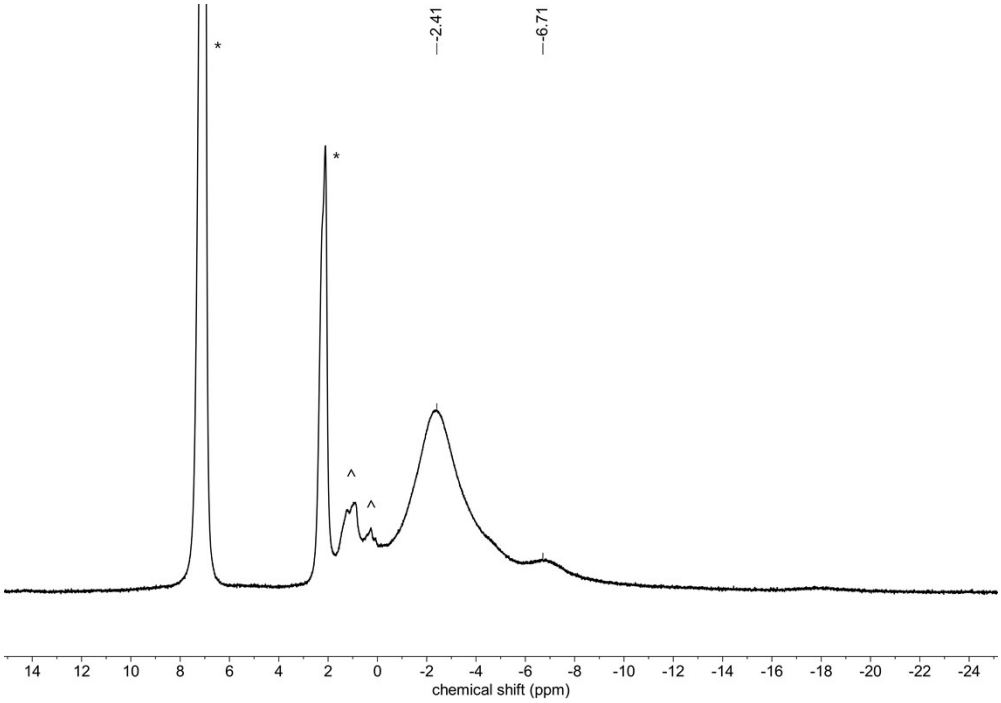

Figure S 15. ^{1}H NMR spectrum (300 MHz, 300 K, toluene-d$_8$) of [({Me$_3$Si}$_2$N)Fe{μ-N^{t}Bu-μ-(N{SiMe$_3$}$_2$)Fe(N{SiMe$_3$}$_2$)], **3** (* toluene-d$_8$, residual *n*-pentane).

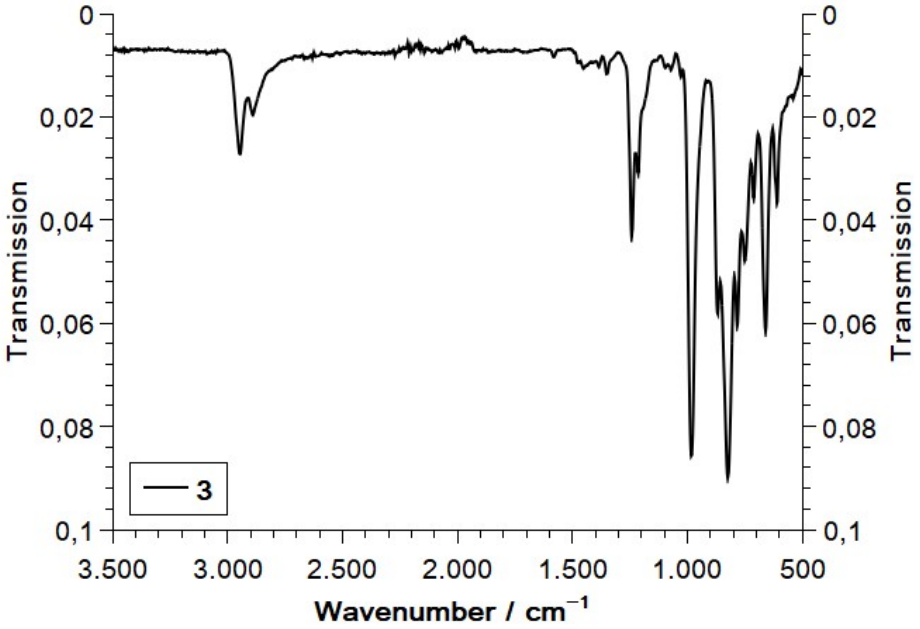

Figure S 16. ATR IR spectrum of solid [({Me_3Si}$_2$N)Fe{μ-N^{t}Bu-μ-(N{$SiMe_3$}$_2$)Fe(N{$SiMe_3$}$_2$)], **3**.

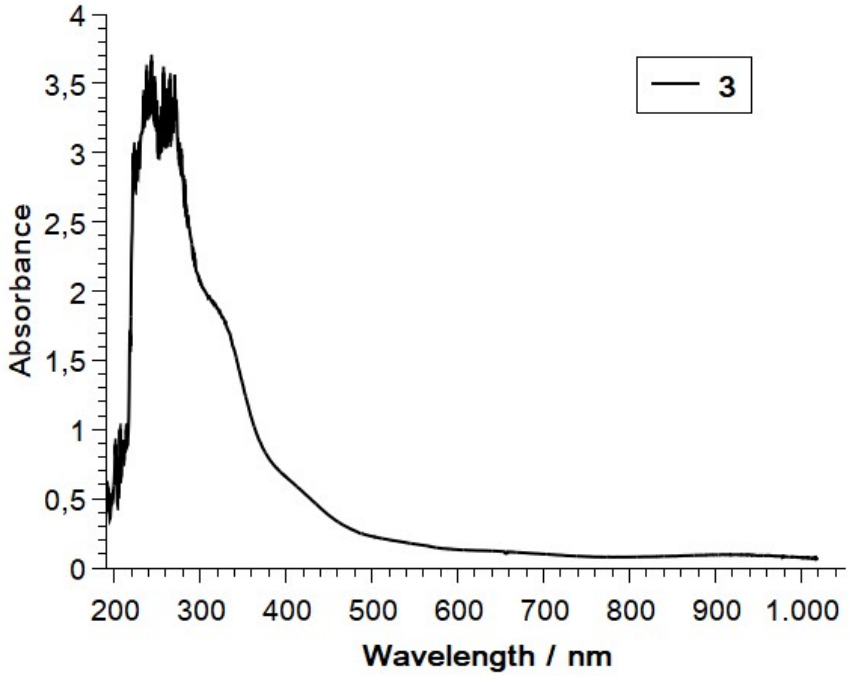

Figure S 17. UV-Vis spectrum of UV-Vis spectrum of [({Me_3Si}$_2$N)Fe{μ-N^{t}Bu-μ-(N{$SiMe_3$}$_2$)Fe(N{$SiMe_3$}$_2$)], **3**, in tetrahydrofuran.

Mössbauer spectroscopy

Mössbauer spectra were recorded with a ^{57}Co source in a Rh matrix using an alternating constant acceleration Wissel Mössbauer spectrometer operated in transmission mode and equipped with a Janis closed-cycle helium cryostat. Isomer shifts are given relative to iron metal at ambient temperature. Simulation of the experimental data was performed with the Mfit program using Lorentzian line doublets: E. Bill, Max-Planck Institute for Chemical Energy Conversion, Mülheim/Ruhr, Germany.

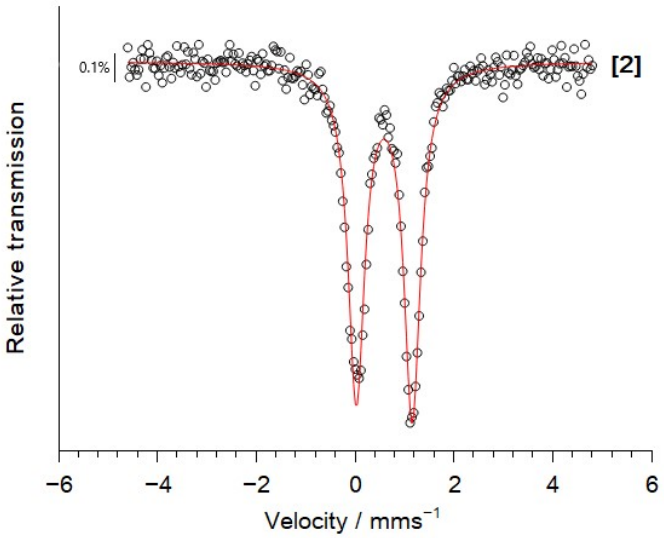

Figure S 18. Mössbauer specrum of solid **2** at 80 K. Parameters for **2**: δ = 0.59 mm s^{-1}, $|\Delta E_Q|$ = 1.13 mm s^{-1}.

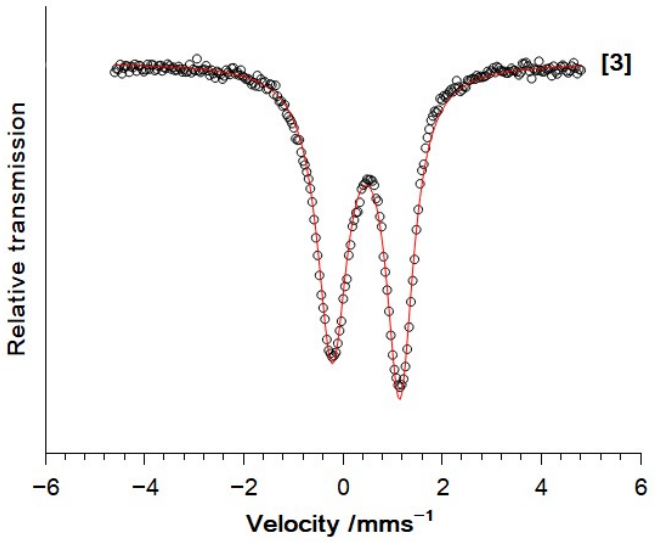

Figure S 19. Mössbauer specrum of solid **3** at 80 K. Parameters for **3**: δ = 0.47 mm s^{-1}, $|\Delta E_Q|$ = 1.36 mm s^{-1}.

X-Ray diffraction analysis and molecular structures

Data for **1** (CCDC 2283997), **2** (CCDC 2283999) and **3** (CCDC 2283998) were collected at 100 K on a Bruker Quest D8 diffractometer using a graphite-monochromated Mo-Kα radiation and equipped with an *Oxford Instrument Cooler Device*. For the irradiation experiment (CCDC 2284001, pre-irradiation. CCDC 2283996, 1 h. CCDC 2284000, 3 h) a new crystal was irradiated directly on the goniometer with blue light (Kessel PR160, LED, 40 W, 390 nm) with the N_2-flow set at 80 K. Data was obtained at 80 K prior irradiation as well as after 1 h and further 2 h of irradiation (3 h total). Longer irradiation was not possible as even after 3 h, substantial degradation of the diffraction pattern and reflex intensity could be seen.

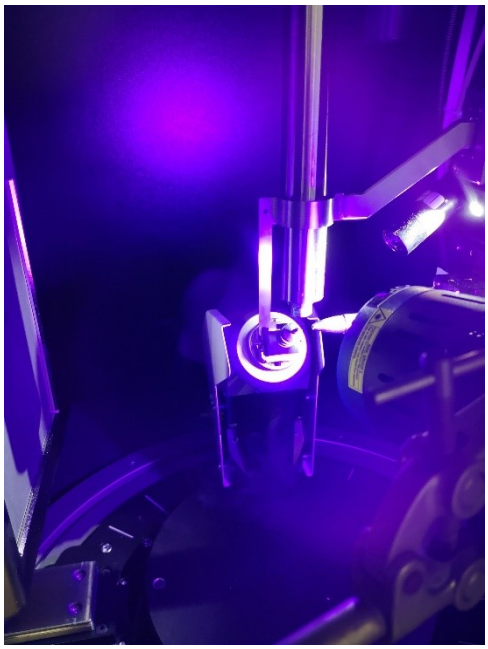

Figure S 20. Photo of the irradiation setting for **1**. Distance between lamp and crystal approximately 15 cm.

The structures were solved using either OLEX SHELXT V2014/1[7] and refined using least-squares procedures on a F^2 with the aid of the program SHELXL-2016/6[8] included in the software package WinGX version 1.63[9] or by CRYSTALS[10]. The Atomic Scattering Factors were taken from *International Tables for X-Ray Crystallography*[11]. All non-hydrogen atoms were refined anisotropically. All hydrogen atoms were refined using a riding model. The absorption correction was introduced using the MULTISCAN and X-Red programs.[12] The molecule drawing was performed with the program DIAMOND (Crystal Impact, Bonn, Germany) with 50% probability displacement ellipsoids for non-hydrogen atoms. Depiction of hydrogen atoms is omitted for clarity.

Crystal data and structure refinements for [Fe{N_3^{t}Bu}($N(SiMe_3)_2$)$_2$], 1.

Empirical formula	$C_{16}H_{45}FeN_5Si_4$
Formula weight	475.78
Temperature/K	100.00
Crystal system	monoclinic
Space group	$P2_1/n$
a/Å	8.7622(2)
b/Å	16.0342(7)
c/Å	20.4887(7)
α/°	90
β/°	101.2450(10)
γ/°	90
Volume/Å^3	2823.29(17)
Z	4
ρ_{calc}g/cm^3	1.119
μ/mm^{-1}	0.714
F(000)	1032.0
Crystal size/mm^3	0.2 × 0.127 × 0.096
Radiation	MoKα (λ = 0.71073)
2Θ range for data collection/°	4.054 to 59.976
Index ranges	−10 ≤ h ≤ 12, −22 ≤ k ≤ 18, −28 ≤ l ≤ 23
Reflections collected	24874
Independent reflections	7466 [R_{int} = 0.0390, R_{sigma} = 0.0494]
Data/restraints/parameters	7466/0/244
Goodness-of-fit on F^2	1.085
Final R indexes [I>=2σ (I)]	R_1 = 0.0328, wR_2 = 0.0798
Final R indexes [all data]	R_1 = 0.0483, wR_2 = 0.0835
Largest diff. peak/hole / e Å^{-3}	0.47/−0.38

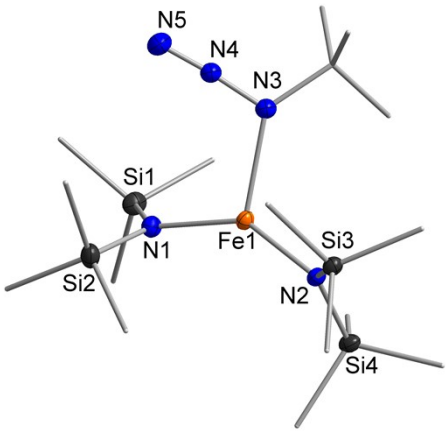

Figure S 21. Molecular structure of [Fe{N_3^{t}Bu}($N(SiMe_3)_2$)$_2$], **1**.

Crystal data and structure refinements for [Fe(κ^2*N*-$N(SiMe_3)SiMe_2CH_2$-NH^tBu)($N(SiMe_3)_2$)], 2.

Empirical formula	$C_{16}H_{45}FeN_3Si_4$
Formula weight	447.76
Temperature/K	100.00
Crystal system	monoclinic
Space group	$P2_1/c$
a/Å	9.3458(4)
b/Å	19.5220(7)
c/Å	15.2414(7)
α/°	90
β/°	106.253(2)
γ/°	90
Volume/Å^3	2669.64(19)
Z	4
ρ_{calc}g/cm^3	1.114
μ/mm^{-1}	0.749
F(000)	976.0
Crystal size/mm^3	0.253 × 0.247 × 0.183
Radiation	MoKα (λ = 0.71073)
2Θ range for data collection/°	4.172 to 60.07
Index ranges	−12 ≤ h ≤ 12, −27 ≤ k ≤ 21, −19 ≤ l ≤ 21
Reflections collected	18947
Independent reflections	7221 [R_{int} = 0.0441, R_{sigma} = 0.0571]
Data/restraints/parameters	7221/7/250
Goodness-of-fit on F^2	1.131
Final R indexes [I>=2σ (I)]	R_1 = 0.0424, wR_2 = 0.1086
Final R indexes [all data]	R_1 = 0.0592, wR_2 = 0.1139
Largest diff. peak/hole / e Å^{-3}	0.78/−0.78

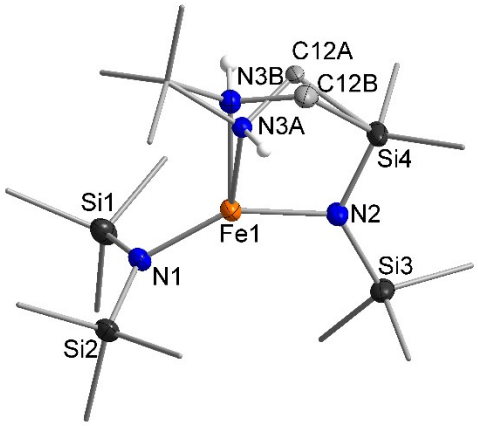

Figure S 22. Molecular structure of [Fe(κ^{2}N-N(SiMe$_3$)SiMe$_2$CH$_2$-NH^{t}Bu)(N(SiMe$_3$)$_2$)], **2**, with the depiction of a disorder of the N3 and C12 Atoms. (ratio 0.76:0.24).

Crystal data and structure refinements for [({Me$_3$Si}$_2$N)Fe(μ-N^{t}Bu-μ-(N{SiMe$_3$}$_2$))Fe(N{SiMe$_3$}$_2$)], **3.**

Empirical formula	$C_{22}H_{63}Fe_2KN_4Si_6$
Formula weight	703.10

Temperature/K	100.00
Crystal system	monoclinic
Space group	$P2_1/c$
a/Å	9.2649(4)
b/Å	14.9686(6)
c/Å	27.6440(11)
α/°	90
β/°	93.938(2)
γ/°	90
Volume/Å^3	3824.7(3)
Z	4
ρ_{calc}g/cm^3	1.221
μ/mm^{-1}	1.073
F(000)	1512.0
Crystal size/mm^3	0.312 × 0.199 × 0.068
Radiation	MoKα (λ = 0.71073)
2Θ range for data collection/°	4.406 to 53.53
Index ranges	−11 ≤ h ≤ 11, −18 ≤ k ≤ 18, −34 ≤ l ≤ 35
Reflections collected	95490
Independent reflections	8137 [R_{int} = 0.0414, R_{sigma} = 0.0185]
Data/restraints/parameters	8137/0/392
Goodness-of-fit on F^2	1.101
Final R indexes [I>=2σ (I)]	R_1 = 0.0284, wR_2 = 0.0632
Final R indexes [all data]	R_1 = 0.0329, wR_2 = 0.0648
Largest diff. peak/hole / e Å^{-3}	0.40/−0.36

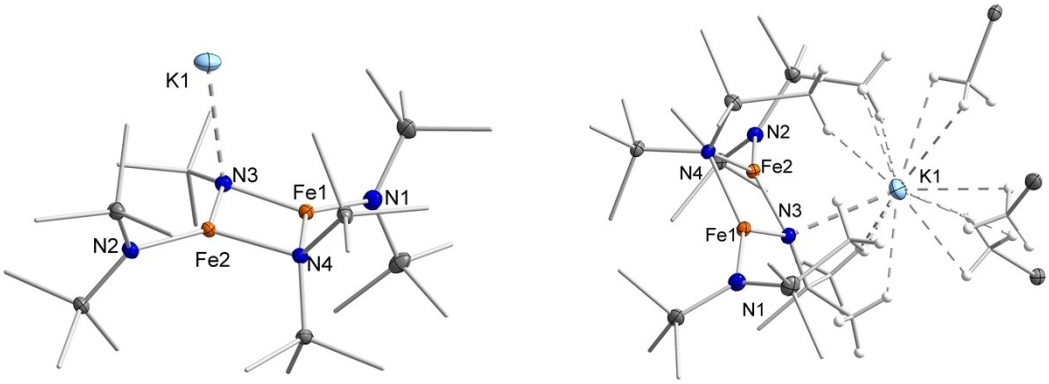

Figure S 23. Molecular structure of [(({Me_3Si}$_2$N)Fe)(μ-N^{t}Bu)(μ-(N{$SiMe_3$}$_2$))] (**3**, (left) and depiction of the K···H interactions with its surroundings (right).

Crystal data and structure refinements for [Fe(N_3^{t}Bu)(N($SiMe_3$)$_2$)$_2$], 1, before and after a total of 1h and 3h of irradiation with a blue LED (390 nm).

Identification code	GWX203_pre	GWX203_1h	GWX203_3h
Empirical formula	$C_{16}H_{45}FeN_5Si_4$	$C_{16}H_{45}FeN_{4.5}Si_4$	$C_{16}H_{45}FeN_{4.31}Si_4$
Formula weight	475.78	468.77	466.08
Temperature/K	80.00	80.00	80.00

Crystal system	monoclinic	monoclinic	monoclinic
Space group	$P2_1/n$	$P2_1/n$	$P2_1/n$
a/Å	8.7573(5)	8.883(4)	8.8341(17)
b/Å	16.0324(7)	16.016(6)	15.935(3)
c/Å	20.4625(11)	20.510(8)	20.441(4)
α/°	90	90	90
β/°	101.169(2)	100.264(11)	100.299(6)
γ/°	90	90	90
Volume/Å^3	2818.5(3)	2871(2)	2831.2(9)
Z	4	4	4
ρ_{calc}g/cm^3	1.121	1.084	1.093
μ/mm^{-1}	0.715	0.701	0.710
F(000)	1032.0	1018.0	1013.0
Crystal size/mm^3	0.14 × 0.105 × 0.034	0.14 × 0.105 × 0.034	0.14 × 0.105 × 0.034
Radiation	MoKα (λ = 0.71073)	MoKα (λ = 0.71073)	MoKα (λ = 0.71073)
2Θ range for data collection/°	4.782 to 51.994	4.738 to 52.098	4.762 to 51.992
Index ranges	-10 ≤ h ≤ 10, -19 ≤ k ≤ 19, -25 ≤ l ≤ 25	-10 ≤ h ≤ 10, -19 ≤ k ≤ 17, -25 ≤ l ≤ 25	-10 ≤ h ≤ 10, -19 ≤ k ≤ 19, -25 ≤ l ≤ 25
Reflections collected	35127	21934	58649
Independent reflections	5531 [R_{int} = 0.0683, R_{sigma} = 0.0547]	5648 [R_{int} = 0.1210, R_{sigma} = 0.1433]	5558 [R_{int} = 0.1714, R_{sigma} = 0.0960]
Data/restraints/ parameters	5531/0/244	5648/27/318	5558/33/318
Goodness-of-fit on F^2	1.075	1.029	1.100
Final R indexes [I>=2σ (I)]	R_1 = 0.0314, wR_2 = 0.0673	R_1 = 0.0694, wR_2 = 0.1597	R_1 = 0.0821, wR_2 = 0.2032
Final R indexes [all data]	R_1 = 0.0458, wR_2 = 0.0698	R_1 = 0.1289, wR_2 = 0.1807	R_1 = 0.1301, wR_2 = 0.2175
Largest diff. peak/hole / e Å^{-3}	0.33/-0.26	0.80/-0.52	1.07/-0.61

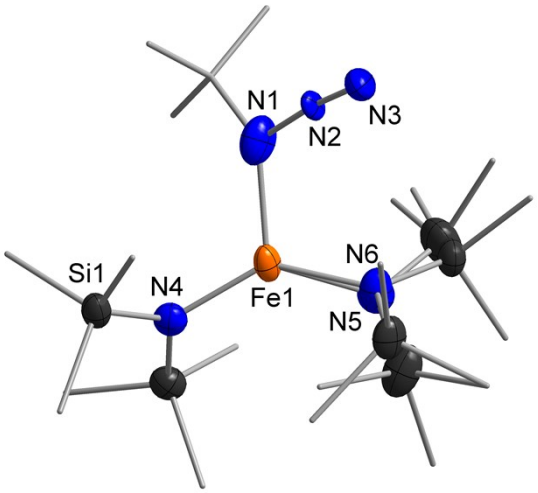

Figure S 24. Molecular structure of Molecular structure of [Fe{N_3*t*Bu}($N(SiMe_3)_2)_2$], **1**, after irradiation (blue LED, 390 nm) of the crystal for a total of 3 h. H atoms are omitted. Depiction of the disorder of one of the $N(SiMe_3)_2$) ligands (ratio 0.8:0.2).

Quantum chemical calculations

The calculations were performed with ORCA v. 5.0.4.[13–16] The structure optimisation for the neutral, putative imido iron complex [**A**] was performed using the the geometric starting points obtained from **1** and removal of its N_2 unit. Geometry optimisation was performed for the singlet, triplet and quintet state using either the r^{2}scan-c3 method or the PBE, PBE0 and TPSSh functionals with the ZORA-def2-SVP/C basis set (def2-TZVP on Fe). All optimized structures were verified as true minima by the absence (N^{imag} = 0) of negative eigenvalues in the harmonic vibrational frequency analysis. Single point calculations were performed for the PBE,[17] PBE0,[18]and TPSSh[19,20] functionals, where scalar relativistic effects were modeled under the Zeroth Order Regular Approximation (ZORA)[21] and using the ZORA-def2-TZVPP[22]basis set. The D4[23] dispersion correction was used. The RI approximation with the related auxiliary basis sets (*SARC/J*)[24] were used to reduce computation time of calculations using the GGA functionals.

For CASSCF/NEVPT2 calculations on [**A**], the geometry obtained from the quintet and the triplet state of the TPSSh calculations was used. In view of geometries of the few known examples of trigonal alkyl (calculated) and aryl imido iron complexes bearing a (silyl)amide ligand set in the literature, which estimate Fe–N bond lengths between 1.7 and 1.8 Å with near-linear Fe–N–R angle,[25,26] the quintet geometry is deemed the most probable and thus focused on in the main manuscript.

The CASSCF/NEVPT2 calculations were then carried out at the triple-ζ level of theory (ZORA-def2-TZVPP, SARC/J, *autoaux, RIJCOSX*), with the active space of CAS[8,7].[27] The active space was chosen as to include d-orbitals and the two imido-nitrogen centered π-orbitals. The electronic structure analysis relates to calculations without state averaging, whereas state-averaging was applied to determine the energies of vertically excited states.

Orbitals were depicted with the help of Chemcraft with a contour value of 0.3.

Multiplicity	Energy (hartree)	Fe–N_{imido}	Fe–N_{imido}–C
PBE			
singlet	-3240.0803442115	1.58	178.3
singlet (unrestricted)	-3240.0796608941	1.59	172.4
triplet	**-3240.0881396815**	1.63	147.0
quintet	-3240.0698809797	1.69	170.5
PBE0			
singlet	-3240.2503050383	1.56	177.6
singlet (unrestricted)	-3240.2434702973	1.60	157.4
triplet	-3240.2792474365	1.67	140.6
quintet	**-3240.2834031718**	1.73	171.5
TPSSh			
singlet	-3242.1745189116	1.57	178.5
singlet (unrestricted)	-3242.1718165222	1.59	165.9
triplet	**-3242.1914473651**	1.63	145.6
quintet	-3242.1825143341	1.70	176.3
r^2SCAN-c3			
singlet	-3222.68952576602	1.59	176.6
singlet (unrestricted)	-3222.69608953512	1.62	152.1
triplet	**-3222.712129**	1.65	144.4
quintet	-3222.708579	1.72	154.4

Table S 1. Energy of the obtained from single point calculations using either the PBE, PBE0, TPSSh functional or the r^2scan-c3 method. Computed M–N_{imido} bond length (Å) and M–N_{imido}–Mes bond angles (°) are given.

		Mulliken		Löwdin	
Multiplicity	**Atom**	**Atomic charge**	**Spin density**	**Atomic charge**	**Spin density**
PBE					
triplet	**Fe**	0.503844	1.929373	-0.206255	1.833271
	N_{imide}	-0.258658	-0.046745	0.134891	0.005477
	N_{amide}	-0.301222	-0.021578	-0.044363	0.020528
	N_{amide}	-0.392384	0.031886	-0.048228	0.058557
quintet	**Fe**	0.568701	3.296775	-0.071062	3.120789
	N_{imide}	0.301944	0.234385	0.114177	0.248311
	N_{amide}	–0.374419	0.098226	-0.056847	0.142654
	N_{amide}	–0.333840	0.178566	-0.053936	0.194024
PBE0					
triplet	**Fe**	0.709001	2.812369	-0.073695	2.635825
	N_{imide}	-0.265649	-0.838980	0.158879	-0.624407
	N_{amide}	-0.345439	-0.024477	-0.078244	0.015431
	N_{amide}	-0.465358	-0.002275	-0.079903	0.029310
quintet	**Fe**	0.753911	4.000840	0.099929	3.811436
	N_{imide}	-0.288361	-0.385701	0.137345	-0.245764
	N_{amide}	-0.445947	0.117461	-0.095692	0.140308
	N_{amide}	-0.433055	0.150357	-0.099761	0.164382
TPSSh					
triplet	**Fe**	0.683301	2.231559	-0.139495	2.099000
	N_{imide}	-0.359436	-0.298800	0.124715	-0.189414
	N_{amide}	-0.395371	-0.034668	-0.065044	0.012462
	N_{amide}	0.496728	0.018456	-0.068689	0.048667
quintet	**Fe**	0.775669	3.587879	0.014760	3.396360
	N_{imide}	-0.370397	0.034324	0.113711	0.093934
	N_{amide}	-0.477486	0.096841	-0.087429	0.139249
	N_{amide}	-0.460483	0.123104	-0.082037	0.156470
r^2SCAN-c3					
triplet	**Fe**	0.665722	2.237534	0.818507	2.129435
	N_{imide}	-0.269577	-0.281250	-0.563680	-0.228876
	N_{amide}	-0.412779	-0.020165	-0.807356	0.019954
	N_{amide}	-0.418883	0.019883	-0.821060	0.059078
quintet	**Fe**	0.792358	3.636900	0.989999	3.404592
	N_{imide}	-0.294843	0.039638	-0.601647	0.075466
	N_{amide}	-0.488041	0.172965	-0.849279	0.197246
	N_{amide}	-0.334908	0.091821	-0.837959	0.143369

Table S 2. Mulliken/Löwdin charges and spin densities of the triplet and quintet states obtained from single point calculations using either the PBE, PBE0, TPSSh functional or the r^2scan-c3 method.

Functional	Spin state	Fe-N_{imide}	Fe-N_{amide}	Fe-N_{amide}
PBE	**triplet**	2.1001	1.1944	1.1364
	quintet	1.8249	1.0067	1.0391
PBE0	**triplet**	1.7870	1.0962	1.0579
	quintet	1.5311	0.9507	0.9778
TPSSh	**triplet**	2.0789	1.1563	1.0952
	quintet	1.7451	0.9778	0.9979
r^2scan-3c	**triplet**	1.9900	1.0372	0.9915
	quintet	1.6356	0.8655	0.8993

Table S 3. Löwdin bond orders of the triplet and quintet states obtained from single point calculations using either the PBE, PBE0, TPSSh functional or the r^2scan-c3 method.

Functional	Spin state	Fe-N_{imide}	Fe-N_{amide}	Fe-N_{amide}
PBE	**triplet**	1.7695	0.8746	0.7427
	quintet	1.6293	0.7398	0.8314
PBE0	**triplet**	1.3805	0.7861	0.6298
	quintet	1.3269	0.7189	0.7693
TPSSh	**triplet**	1.6538	0.7780	0.6148
	quintet	1.4757	0.6530	0.6810
r^2scan-3c	**triplet**	1.4916	0.9048	0.8895
	quintet	1.3133	0.8426	0.9545

Table S 4. Mayer bond orders of the triplet and quintet states obtained from single point calculations using either the PBE, PBE0, TPSSh functional or the r^2scan-c3 method.

CASSCF calculations

For the CASSCF/NEVPT2 calculations the geometry of the linear quintet and bent triplet state obtained TPSSh functional was chosen (see Table S1). The active space consists of the 5 d-orbitals an the two π-interacting p_N-orbitals. Inclusion of the σ-N_p interaction yields no significant change in spin-state ordering or population of the configurations, but less informative orbital interactions. It was thus excluded.

Quintet Geometry (TPSSh, Fe–N 1.70 Å, Fe–N–^{t}Bu 176°)

LOWEST ROOT (ROOT 0, MULT 5) = -3238.177705037 Eh -88115.295 eV

State	Root	Mult.	ΔE/a.u.	ΔE/eV	ΔE/cm^{-1}
1:	0	3	0.012932	0.352	2838.3
2:	1	3	0.024263	0.660	5325.1
3:	1	5	0.027924	0.760	6128.7
4:	2	3	0.041749	1.136	9162.8
5:	0	1	0.052986	1.442	11629.1
6:	2	5	0.062974	1.714	13821.1
7:	2	1	0.074096	2.016	16262.1
8:	1	1	0.078962	2.149	17330.2
9:	3	3	0.080129	2.180	17586.3
10:	4	3	0.080708	2.196	17713.4

Figure S 25. NEVPT2 transition energies of [**A**] with regards to the quintet ground state obtained from state-averaged ZORA-def2-TZVPP/CASSCF(8,7) calculations.

Quintet state (root 0, multiplicity 5)

	118	119	120	121	122	123	124
	-0.44974	-0.37147	0.25867	-0.24473	-0.26114	-0.26898	-0.01763
	1.97335	1.54910	1.02530	1.00022	1.00013	0.99971	0.45219
	--------	--------	--------	--------	--------	--------	--------
0 Fe s	0.0	0.0	0.0	0.0	0.0	1.9	0.0
0 Fe pz	0.2	1.9	0.0	0.9	0.1	0.2	0.1
0 Fe px	1.4	0.6	0.2	0.6	0.2	0.1	0.1
0 Fe py	1.7	1.1	0.2	0.2	0.1	0.1	0.1
0 Fe dz2	1.4	31.8	6.7	13.3	1.0	10.5	31.9
0 Fe dxz	1.1	4.0	4.9	54.2	5.5	20.2	3.4
0 Fe dyz	5.8	0.3	27.9	15.3	45.2	0.4	0.2
0 Fe dx2y2	8.9	0.0	42.8	2.7	42.4	3.3	0.0
0 Fe dxy	0.9	12.8	4.3	6.2	0.1	59.1	12.6
1 N pz	3.6	18.8	0.4	0.2	0.1	0.4	19.2
1 N px	29.1	5.7	3.8	0.2	0.1	0.5	6.0
1 N py	33.3	13.0	4.6	0.1	0.0	0.2	14.1

Figure S 26. Reduced Löwdin population analysis of active space in CASSCF(8,7) of quintet **A**.

0.67123 [111]: 2211110
0.17975 [96]: 2111111
0.12198 [81]: 2011112
0.01992 [53]: 1121111
0.00321 [21]: 1021112

Figure S 27. Configuration of ground state of of quintet **A** as obtained by CASSCF(8,7).

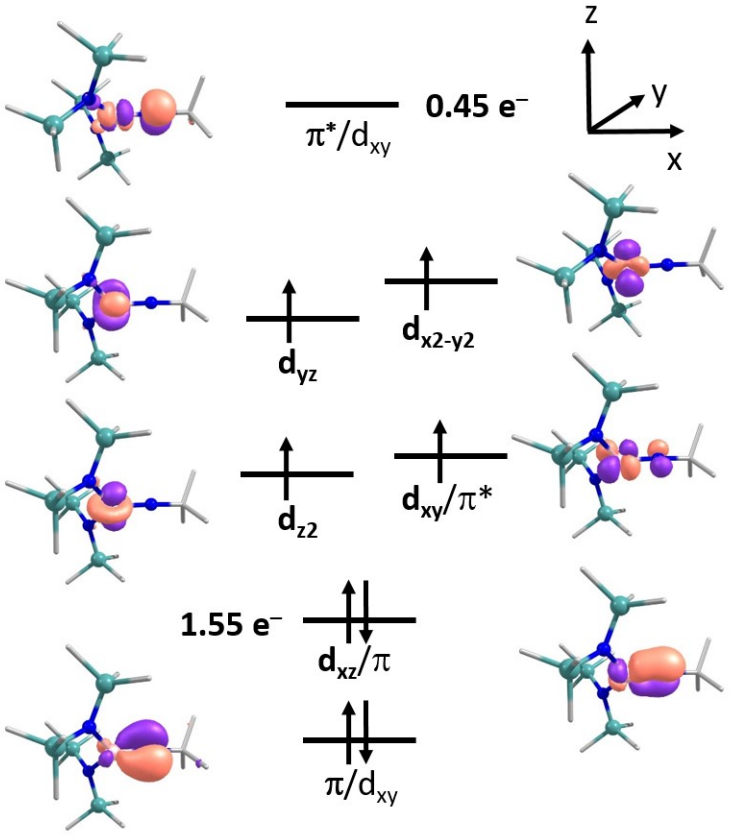

Figure S 28. Orbital scheme of the active space from CASSCF(8,7) of quintet **A**.

Triplet Geometry (TPSSh, Fe–N 1.63, Fe–N–^{t}Bu 145.6°)

```
LOWEST ROOT (ROOT 0, MULT 3) =  -3238.179705217 Eh -88115.349 eV
STATE ROOT MULT  ΔE/a.u.     ΔE/eV    ΔE/cm**-1
   1:   1    3   0.013071     0.356   2868.7
   2:   0    5   0.022514     0.613   4941.4
   3:   2    3   0.026141     0.711   5737.2
   4:   1    5   0.036787     1.001   8073.8
   5:   0    1   0.050521     1.375  11088.0
   6:   1    1   0.059976     1.632  13163.1
   7:   2    1   0.064963     1.768  14257.8
   8:   4    1   0.079943     2.175  17545.4
   9:   3    1   0.080096     2.180  17579.1
  10:   2    5   0.081746     2.224  17941.3
  11:   3    3   0.089534     2.436  19650.5
  12:   4    3   0.098539     2.681  21626.7
```

Figure S 29. NEVPT2 transition energies of [**A**] with regards to the triplet ground state obtained from state-averaged ZORA-def2-TZVPP/CASSCF(10,8) calculations.

Triplet state (root 0, multiplicity 3)

		114	115	116	117	118	119
		-0.39505	-0.38122	-0.34823	-0.59145	-0.59506	-0.43756
		2.00000	2.00000	2.00000	1.98801	1.98510	1.81294
0	Fe dz2	0.0	0.1	0.1	0.9	8.1	7.6
0	Fe dyz	0.1	0.9	0.1	31.4	14.4	0.9
0	Fe dx2y2	0.0	0.9	0.1	41.1	1.7	14.2
0	Fe dxy	0.4	0.1	0.1	7.1	1.5	19.4
1	N s	0.0	0.2	0.0	0.3	9.4	0.1
1	N px	0.0	1.5	0.0	1.5	12.1	19.0
1	N py	0.2	0.4	0.2	2.5	20.5	27.6
2	N pz	5.9	0.9	0.0	0.4	0.1	0.1
2	N px	1.1	2.0	19.2	1.6	3.5	0.3
2	N py	2.9	8.7	8.9	0.0	0.0	0.0
3	N pz	5.2	5.2	0.5	0.4	0.9	0.0
3	N px	1.6	4.7	14.1	1.9	6.0	0.0
3	N py	1.8	8.3	4.7	0.1	0.4	0.0

		120	121	122	123	124	125
		-0.40197	-0.14827	-0.14444	0.08287	0.13335	0.11450
		1.77537	1.01630	0.99993	0.23155	0.19080	0.00000
0	Fe s	0.0	0.1	0.0	0.0	0.0	5.2
0	Fe dz2	0.2	13.8	53.0	0.4	14.1	0.4
0	Fe dxz	40.4	4.8	0.2	50.4	0.3	0.1
0	Fe dyz	0.0	12.7	29.2	0.0	3.6	0.1
0	Fe dx2y2	0.2	4.3	14.2	0.1	23.7	0.2
0	Fe dxy	1.9	52.4	0.0	2.9	15.1	0.5
1	N pz	44.3	0.3	0.0	32.5	0.2	0.0
1	N px	0.2	0.0	0.0	0.1	15.6	0.0
1	N py	1.1	3.3	0.0	1.3	13.9	0.2
35	H s	0.0	0.0	0.0	0.0	0.0	5.2

Figure S 30. Reduced Löwdin population analysis of active space in CASSCF(10,8) of triplet **A**.

```
ROOT   0:  E=   -3232.6650269791 Eh
      0.76049 [   727]: 22221100
      0.04733 [   700]: 22201120
      0.04402 [   667]: 22111111
      0.04136 [   717]: 22211110
      0.03360 [   634]: 22021102
      0.02811 [   687]: 22121101
      0.00770 [   607]: 22001122
      0.00410 [   589]: 21212110
      0.00374 [   617]: 22011112
      0.00317 [   647]: 22101121
      0.00310 [   553]: 21122101
```

Figure S 31. Configuration of ground state of of triplet **A** as obtained by CASSCF(10,8).

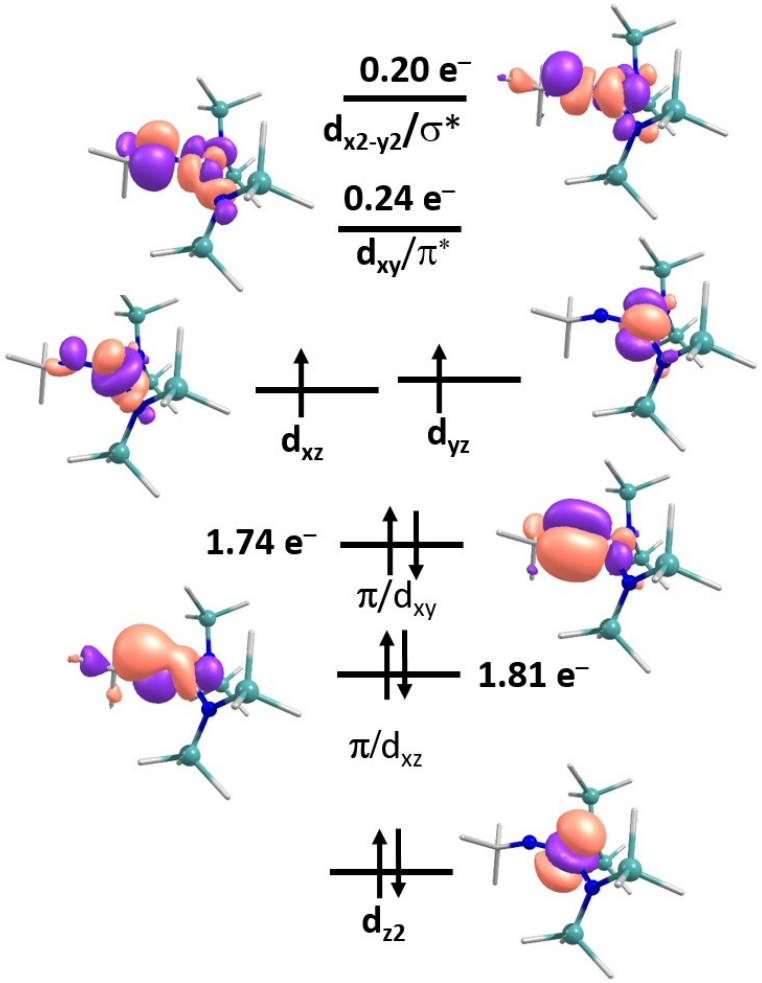

Figure S 32. Orbital scheme of the active space from CASSCF(8,7) of triplet **A**.

XYZ-Coordinates of quintet [A] (from TPSSh) used for the CASSCF calculations

Fe	1.168916000	12.033158000	12.538823000
N	2.298235000	12.685449000	13.625608000
N	-0.047040000	10.682108000	12.985368000
N	1.197895000	12.451991000	10.719417000
Si	2.817789000	12.610433000	10.034702000
C	3.542748000	14.312677000	10.423687000
C	3.925831000	11.263374000	10.768352000

C	2.793078000	12.344074000	8.159650000
Si	-0.263115000	12.998224000	9.898109000
C	-0.812981000	11.837994000	8.510238000
C	0.021906000	14.724998000	9.166073000
C	-1.680489000	13.134651000	11.137923000
Si	0.384833000	9.070373000	12.406182000
C	0.511275000	9.024815000	10.524420000
C	-0.896919000	7.770792000	12.911150000
C	2.056516000	8.580679000	13.156118000
Si	-1.008312000	10.970753000	14.434949000
C	-0.300843000	10.054495000	15.935399000
C	-1.028573000	12.826846000	14.821347000
C	-2.809242000	10.443072000	14.188449000
C	3.185489000	13.216420000	14.603136000
C	2.911837000	14.726650000	14.786509000
C	2.921401000	12.467199000	15.932176000
C	4.650737000	12.987923000	14.166813000
H	-0.022333000	11.667792000	7.770181000
H	-1.675732000	12.273493000	7.987025000
H	-1.116970000	10.863924000	8.909641000
H	2.977939000	15.105607000	9.917920000
H	4.592451000	14.388266000	10.109114000
H	3.492154000	14.502264000	11.502961000
H	3.953017000	11.318074000	11.863614000
H	4.956747000	11.368524000	10.403133000
H	3.568727000	10.265262000	10.483370000
H	3.074211000	15.260643000	13.843630000
H	3.581130000	15.148918000	15.546683000
H	1.875203000	14.890289000	15.101337000
H	1.889533000	12.622123000	16.263655000
H	3.600757000	12.840751000	16.708298000
H	3.090085000	11.392927000	15.801335000
H	0.299768000	15.437652000	9.953586000
H	-0.898261000	15.090088000	8.689099000
H	0.814352000	14.736228000	8.407530000
H	2.422417000	11.340315000	7.915724000
H	3.815396000	12.429099000	7.765725000
H	2.171896000	13.075050000	7.628297000
H	-0.336425000	8.965949000	15.801229000
H	-0.870963000	10.295096000	16.843325000
H	0.745047000	10.336313000	16.106444000
H	-0.488296000	9.038234000	10.071965000
H	1.016011000	8.105461000	10.197947000
H	1.062832000	9.887857000	10.135957000
H	-0.022121000	13.264206000	14.839849000
H	-1.480953000	12.989121000	15.809626000
H	-1.629286000	13.379347000	14.088742000
H	-1.858287000	12.173921000	11.634961000
H	-2.601540000	13.434533000	10.619362000
H	-1.473658000	13.891752000	11.905859000
H	4.853402000	11.916361000	14.061570000

H	5.338464000	13.402643000	14.914491000
H	4.847631000	13.474518000	13.205495000
H	-1.017687000	7.679316000	13.997316000
H	-0.571142000	6.792514000	12.530854000
H	-1.878478000	7.988447000	12.472190000
H	2.846305000	9.289369000	12.874212000
H	2.370187000	7.581493000	12.823645000
H	1.994763000	8.572338000	14.252188000
H	-3.235685000	10.911597000	13.292394000
H	-3.408853000	10.761730000	15.052573000
H	-2.916722000	9.357278000	14.089032000

XYZ-Coordinates of triplet [A] (from TPSSh) used for the CASSCF calculations

Fe	0.000000000	0.000000000	0.000000000
N	1.629728000	0.000000000	0.000000000
N	-0.853518000	-0.776373000	1.397214000
N	-0.901027000	0.590039000	-1.473544000
Si	-0.591851000	-0.091710000	-3.073509000
C	1.026275000	0.609842000	-3.758459000
C	-0.511267000	-1.977960000	-3.017383000
C	-1.995122000	0.330357000	-4.275406000
Si	-1.696415000	2.156961000	-1.239815000
C	-3.557524000	1.991942000	-1.530312000
C	-0.971901000	3.462766000	-2.403810000
C	-1.452269000	2.777366000	0.527527000
Si	-1.869558000	-2.186817000	1.024736000
C	-3.111206000	-1.779185000	-0.335138000
C	-2.910391000	-2.728875000	2.514250000
C	-0.767400000	-3.643886000	0.537971000
Si	-0.418538000	-0.286645000	3.050357000
C	0.375881000	-1.726199000	3.993621000
C	0.796434000	1.157241000	3.069652000
C	-1.964698000	0.278943000	3.986175000
C	2.820083000	-0.801524000	-0.144617000
C	3.962313000	0.166538000	-0.526309000
C	3.114207000	-1.458754000	1.220818000
C	2.673255000	-1.898462000	-1.213547000
H	-3.796945000	1.667617000	-2.549093000
H	-4.051182000	2.958392000	-1.358047000
H	-3.987968000	1.262277000	-0.833415000
H	0.911731000	1.670437000	-4.014760000
H	1.346830000	0.075182000	-4.662781000
H	1.824706000	0.536994000	-3.010642000
H	0.189111000	-2.342446000	-2.260986000
H	-0.183919000	-2.363965000	-3.992762000
H	-1.496576000	-2.407448000	-2.800605000
H	3.754796000	0.640917000	-1.491780000
H	4.911702000	-0.378462000	-0.600271000
H	4.061827000	0.952633000	0.229850000
H	3.220619000	-0.701730000	2.004949000
H	4.045187000	-2.036557000	1.163966000

H	2.296511000	-2.134204000	1.493094000
H	0.103998000	3.581686000	-2.221318000
H	-1.454567000	4.434305000	-2.229517000
H	-1.108804000	3.209278000	-3.461999000
H	-2.945350000	-0.101416000	-3.936425000
H	-1.763807000	-0.104723000	-5.257885000
H	-2.139447000	1.407790000	-4.418205000
H	-0.267297000	-2.613441000	4.026318000
H	0.577167000	-1.423946000	5.030799000
H	1.330428000	-2.019723000	3.541255000
H	-3.895182000	-1.123753000	0.066147000
H	-3.592511000	-2.695395000	-0.703076000
H	-2.643992000	-1.259561000	-1.176232000
H	1.685353000	0.958733000	2.462125000
H	1.112047000	1.338184000	4.107055000
H	0.333599000	2.077431000	2.695495000
H	-1.823536000	2.053981000	1.263189000
H	-2.006906000	3.716741000	0.663697000
H	-0.394883000	2.976376000	0.741352000
H	1.883024000	-2.600841000	-0.928899000
H	3.613192000	-2.456463000	-1.308785000
H	2.428361000	-1.465380000	-2.187927000
H	-2.325380000	-2.968868000	3.409214000
H	-3.454992000	-3.638529000	2.223372000
H	-3.656950000	-1.971279000	2.781370000
H	-0.196685000	-3.425727000	-0.371824000
H	-1.362736000	-4.548467000	0.353591000
H	-0.051842000	-3.865527000	1.340737000
H	-2.520592000	1.031444000	3.412436000
H	-1.663291000	0.739908000	4.937158000
H	-2.647395000	-0.545678000	4.217209000

References

[1] http://supramolecular.org.

[2] Brynn Hibbert, D.; Thordarson, P. *Chem. Commun.* **2016**, *52*, 12792–12805.

[3] Evans, D. F. *J. Chem. Soc.* **1959**, 2003.

[4] Schubert, E. M. *J. Chem. Educ.* **1992**, *69*, 62.

[5] Andersen, R. A.; Faegri, K.; Green, J. C.; Haaland, A.; Lappert, M. F.; Leung, W. P.; Rypdal, K. *Inorg. Chem.* **1988**, *27*, 1782–1786.

[6] Bottaro, J. C.; Penwell, P. E.; Schmitt, R. J. *Synth. Commun.* **1997**, *27*, 1465–1467.

[7] Sheldrick, G. M. *Acta Cryst. A* **2015**, *71*, 3–8.

[8] Sheldrick, G. M. *Acta. Crystallogr. C* **2015**, *71*, 3–8.

[9] Farrugia, L. J. *J. Appl. Crystallogr.* **1999**, *32*, 837–838.

[10] Betteridge, P. W.; Carruthers, J. R.; Cooper, R. I.; Prout, K.; Watkin, D. J. *J. Appl. Crystallogr.* **2003**, *36*, 1487.

[11] Fueß, H., Ed. *International tables for crystallography*, 1. online ed.; Springer: Berlin, 2006.

[12] SADABS-2016/2. *Bruker*, 2016.

[13] Neese, F. *WIREs Comput Mol Sci* **2022**, *12*.

[14] Neese, F. *WIREs Comput Mol Sci* **2018**, *8*.

[15] Neese, F. *WIREs Comput Mol Sci* **2012**, *2*, 73–78.

[16] Neese, F.; Wennmohs, F.; Becker, U.; Riplinger, C. *J. Chem. Phys.* **2020**, *152*, 224108.

[17] Perdew, J. P.; Ernzerhof, M.; Burke, K. *J. Chem. Phys.* **1996**, *105*, 9982–9985.

[18] Adamo, C.; Barone, V. *J. Chem. Phys.* **1999**, *110*, 6158–6170.

[19] Tao, J.; Perdew, J. P.; Staroverov, V. N.; Scuseria, G. E. *Phys. Rev. Lett.* **2003**, *91*, 146401.

[20] Staroverov, V. N.; Scuseria, G. E.; Tao, J.; Perdew, J. P. *J. Chem. Phys.* **2003**, *119*, 12129–12137.

[21] van Wüllen, C. *J. Chem. Phys.* **1998**, *109*, 392–399.

[22] Weigend, F.; Ahlrichs, R. *Phys. Chem. Chem. Phys.* **2005**, *7*, 3297–3305.

[23] Caldeweyher, E.; Ehlert, S.; Hansen, A.; Neugebauer, H.; Spicher, S.; Bannwarth, C.; Grimme, S. *J. Chem. Phys.* **2019**, *150*, 154122.

[24] Weigend, F. *Phys. Chem. Chem. Phys.* **2006**, *8*, 1057–1065.

[25] Reith, S.; Demeshko, S.; Battistella, B.; Reckziegel, A.; Schneider, C.; Stoy, A.; Lichtenberg, C.; Meyer, F.; Munz, D.; Werncke, C. G. *Chem. Sci.* **2022**, *13*, 7907–7913.

[26] Yang, P.-C.; Yu, K.-P.; Hsieh, C.-T.; Zou, J.; Fang, C.-T.; Liu, H.-K.; Pao, C.-W.; Deng, L.; Cheng, M.-J.; Lin, C.-Y. *Chem. Sci.* **2022**, *13*, 9637–9643.

[27] Roos, B. O.; Taylor, P. R.; Sigbahn, P. E. *Chem. Phys.* **1980**, *48*, 157–173.